# *In Situ* Nanoscale Characterization of Redox Processes in Ceria Zirconia

*Ruigang Wang,[*, **] Peter A. Crozier,[*, **] Renu Sharma,[*, **] and James B. Adams[*]*

[*]*School of Materials, Arizona State University, Tempe, AZ 85287-1704*
[**]*Center for Solid State Science, Arizona State University, Tempe, AZ 85287-1704*

## Introduction

The ability of cerium oxides to reversibly form +3 and +4 valence oxides ($CeO_2$ and $Ce_2O_3$) can lead to excellent oxygen storage capacity (OSC). Oxygen vacancy ordering may inhibit the reversible nature of the redox process [1]. It is well-known that doping with zirconia not only improves the life of the redox cycles but also lowers the reduction temperature [2]. Therefore nanoscale ceria-zirconia particles have been widely used in automobile three-way catalysts to adjust the local oxygen environment in order to decrease pollutants from the engine exhaust. However, the complex nature of ceria-zirconia solid solutions can lead to the formation of two types of heterogeneity, especially at the nanometer level: chemical compositional heterogeneity ($x$ in $Ce_xZr_{1-x}O_2$, $0 \leq x \leq 1$) and structural heterogeneity. Some recent reports [3, 4] have pointed out that the pyrochlore-related phases ($Ce_2Zr_2O_{7+x}$, $0 \leq x \leq 1$) formed after high-temperature reduction treatment might be the active phases for the onset of low-temperature reduction for successive cycles. A detailed description of the active phases and phase transformations during redox cycles is necessary in order to develop a fundamental understanding of the redox properties of this system. For example, the role of oxygen vacancy ordering and/or pyrochlore-related phases on the low-temperature reducibility should be clarified. Consequently structural and chemical characterization should be performed at the nanometer level to identify the active phases, especially under reaction conditions. However, the redox behavior of Ce is difficult to observe, as partially reduced cerium oxide is unstable at low-temperatures and/or in high oxygen partial pressure. For this reason, in our present study, we have undertaken a detailed *in situ* transmission electron microscopy (TEM) study of the dynamic nanostructural and nanochemical changes that take place in ceria zirconia during redox processes.

## Experimental section

### *Sample preparation*

In order to achieve an intimate mixture (well mixed solid solution nanoparticles) of cerium and zirconium precursor, intensive synthesis routes have been investigated, especially some wet chemical methods [5-8]. In our work, we prepared high surface area samples of $50\%CeO_2 50\%ZrO_2$ ($Ce_{0.5}Zr_{0.5}O_2$) using a spray freezing method [9]. Samples were calcined at $500^0C$ for 5h in air and then subjected to an activation process consisting of one redox cycle (reduced in $H_2$ at $1000^0C$ for 2.75 h and subsequently re-oxidized in air). The following procedure was performed for the standard cleaning and redox treatment ("activation step"): $20^0C$ for 1h, $10^0C$/min up to $300^0C$, hold at $300^0C$ for 5h, $10^0C$/min down to $150^0C$, hold at $150^0C$ for 5h, $2^0C$/min up to $1000^0C$, hold at $1000^0C$ for 2.75h, $5^0C$/min down to $20^0C$, hold at $20^0C$ for 1h, all in $5\%H_2$/He; and then the sample was held in glass bottle for 1 week in air at room temperature before further characterization.

### Ex situ characterization of average redox behavior

The average redox activity of the material was determined *ex situ* by thermalgravimetric analysis (TGA). The TGA consisted of heating the sample under $5\%H_2/He$ atmosphere from $150^0C$ to $1000^0C$, the cleaning, heating and cooling procedures were exactly the same as the "activation step" mentioned above. The negative of differential mass with respect to temperature (-dM/dT) was plotted with respect to temperature to visualize the reduction process during the ramp up period. The total mass loss due to reduction was calculated from the mass determined just before the start of the cool step.

### In situ characterization of redox behavior of individual nanoparticles

*In situ* TEM nanocharacterization was performed to follow the redox behavior of individual nanoparticles. We have used an environmental scanning transmission electron microscopy (ESTEM) Tecnai F20, operated at 200KeV, equipped with a Gatan imaging filter (GIF) and annular dark-field detector. Ceria zirconia powder was dispersed over Pt grids and loaded into the microscope in a Gatan heating holder. The samples were heated in 1.5 Torr of dry $H_2$ and the temperature was adjusted so that observations could be made both above and below the reduction temperature. Time and temperature resolved atomic resolution images and energy-loss spectra were recorded to follow the structural and chemical changes of individual nanoparticles during the reduction in $H_2$. Energy-loss spectroscopy (EELS) was used to detect redox activity in individual nanograins using the procedure described below. The elemental profile of individual nanocrystallites was obtained by using a nanometer beam in STEM mode and recording EEL spectra for every 1 or 2 nm step (EELS line scans) from individual particles. The EELS line scans were processed to determine the variation in Ce/Zr atomic ratio between different nanoscale grains and within individual nanoparticles.

## Results and discussion

### Synthesis and ex situ characterization of nanoscale ceria zirconia powder

X-ray diffraction analysis (not shown) indicated that the solid solution had a fluorite-like structure and a particles size of about 30nm after $1000^0C$ reduction activation treatment. Figure 1 shows a typical TGA mass loss derivative profiles (-dM/dT) for the activated $Ce_{0.5}Zr_{0.5}O_2$. The profile shows the presence of two peaks suggesting that most of the reduction takes place at 448 and $510^0C$ as determined by a standard Gaussian peak fitting to the data. It is also noted that the mass loss (reduction) starts between $250^0C$ to $300^0C$, indicating that these nanopowders have good low-temperature reducibility. Compared with pure $CeO_2$ (~25nm), this $Ce_{0.5}Zr_{0.5}O_2$ sample shows much higher reduction fraction ($Ce_{0.5}Zr_{0.5}O_2$: 72%; $CeO_2$: 40%) and lower reduction temperature ($Ce_{0.5}Zr_{0.5}O_2$: $448^0C$; $CeO_2$: $757^0C$).

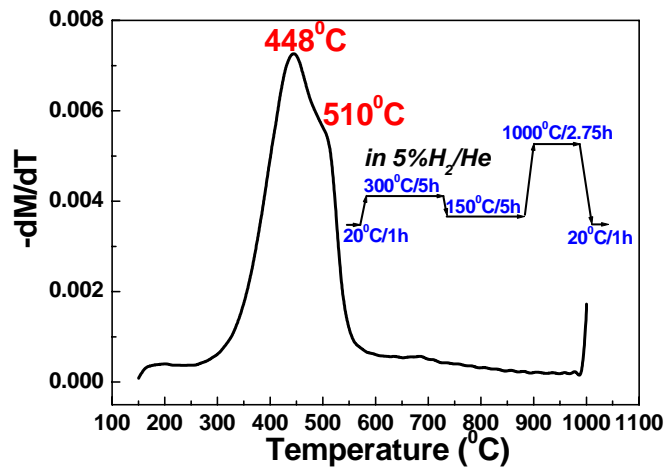*Figure 1: TGA characterization of reduction kinetics in $Ce_{0.5}Zr_{0.5}O_2$ sample. Inserted is thermal profile of the "activation step" and ex situ TGA experiment.*

### *Determining nanoscale heterogeneity and oxidation state of individual nanoparticles*

E*x situ* characterization provided the information about average reduction temperature and total reduction fraction for these nanoscale powders. But *in situ* nanoscale characterization is necessary to get more specific structural and chemical information at the nanometer level. In principle, we can use *in situ* high resolution electron microscope (HREM) images and EELS to determine the most active components of the powders.

Figure 2 shows the Z-contrast STEM image (a) and compositional variation (b) within one individual nanoparticle. The EELS nanoanalysis revealed ~10 - 15% composition variation between individual particles (24 particles were investigated) and a larger variation within some particles (not shown). Structural and chemical heterogeneity at the nanometer level between individual particles can result in different redox behavior between them, in which case it is critically important to distinguish their redox behavior with respect to their composition and structure. Within grains, this nanoscale heterogeneity can produce strain caused by lattice mismatch, which may also play an important role during redox processes.
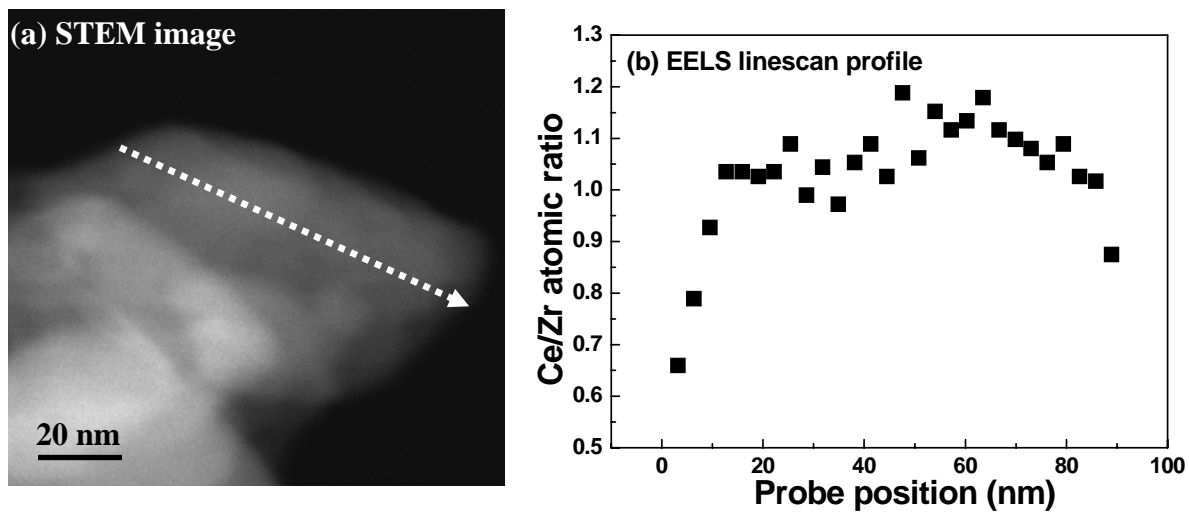


*Figure 2: STEM image (a), chemical profile (b) from EELS linescan within one individual nanoparticle*

*In situ* EELS can be used to monitor the change in Ce oxidation state during reduction. Figure 3 shows energy-loss spectra recorded from a pure ceria nanoparticle under two different conditions: before reduction (room temperature) and under reducing conditions (at $700^{\circ}C$ in 0.5 Torr of $25\%H_2/75\%N_2$). Two important changes take place in the $M_5$ and $M_4$ lines of the spectra when reduction occurs (Figure 3 a and b). First, note the shoulders on the high energy-loss side for $Ce^{4+}$; secondly the reversal of the $M_5/M_4$ edge intensity height between $Ce^{4+}$ and $Ce^{3+}$; i.e. $M_5$ is higher than $M_4$ for high-temperature spectra and $M_5$ is lower than $M_4$ for spectra collected at low-temperature. The change in the relative height of the peaks at the beginning of Ce $M_{4,5}$ edge in the energy-loss spectrum is representative of a transformation of the Ce oxidation state from +4 to +3. Moreover Ce $M_5/M_4$ integrated-peak intensity ratios can be used to quantitatively determine the Ce oxidation state. This makes it possible to determine the redox activity of individual nanoparticles *in situ* and correlate this activity to particle structure and chemistry. For calibration purposes, we have determined $M_5/M_4$ ratio for $CeF_3$ with +3 oxidation state and $CeO_2$ with +4 oxidation state to be 0.796 for 0.672, respectively using low electron dose in order to avoid electron radiation effects. These values are used to determine the Ce oxidation state in the ceria zirconia systems during *in situ* redox cycles.
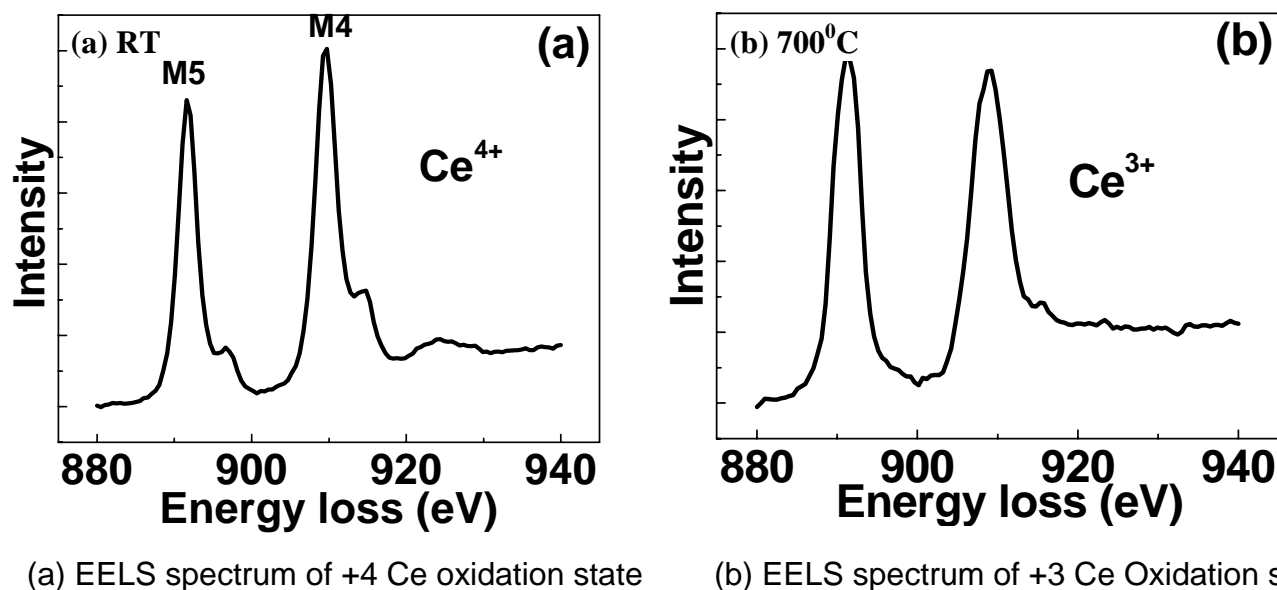


(a) EELS spectrum of +4 Ce oxidation state    (b) EELS spectrum of +3 Ce Oxidation state

*Figure 3: In situ detection of Ce oxidation state at nanometer level using electron energy loss spectroscopy (EELS). Change in relative area of peaks at the beginning of Ce $M_{4,5}$ edge can be used for in situ determination of Ce oxidation state with nanometer resolution.*

Figure 4a and 4b show *in situ* HREM images and associated EELS spectra of two nanoparticles recorded at elevated temperature from $486^{0}C$ to $586^{0}C$ in 1.5 Torr dry $H_2$ respectively. It is clear from the Ce white-lines (insets) that there is a significant difference in the effect of reducing environment on the oxidation state changes of these two nanoparticles. For the fully reduced particle, the oxidation state changed from +3.8 to +4, then down to +3, which means $Ce^{4+}$ was fully reduced to $Ce^{3+}$ under this condition (Figure 4c). The reason for the initial oxidation state being +3.8 is because this sample was activated, *ex situ,* at high temperature ($1000^{0}C$) in a reducing atmosphere ($5\%H_2/He$, 1 atmosphere gas pressure). Therefore the Ce oxidation state in this nanoparticle is a mixture of +3 and +4 valence. According to *ex situ* TGA observations, this sample reduced at $448^{0}C$ (main peak) and $510^{0}C$

(shoulder) [9]. (Since there is much lower $H_2$ gas pressure in TEM environment cell in comparison to *ex situ* experiment, it is reasonable that the reduction temperature *in situ* is higher than *ex situ* reduction shown in TGA experiment above). The oxidation state of the second particle changed very slightly confirming it was stable and relatively inactive.

The reduction process can trigger the formation of ordered oxygen vacancy or pyrochlore-related structures which both will contain Ce in +3 oxidation states. Although these two-types of phases have Ce in a similar oxidation state (+3 or mixed +3 and +4) their reducibility may be widely different. The oxygen vacancy ordering is believed to reduce oxygen mobility (ordered oxygen vacancy structures may be resistant to release or storage of more oxygen) and thus result in higher reduction temperature. However, pyrochlore-related phases may have high activity at low-temperature [10-13]. Therefore, it is necessary to distinguish and identify these structures by further *in situ* experiments, as some of these forms are not stable under *ex situ* conditions. But the key point here is that with *in situ* EELS, it is possible to identify the most active individual nanoparticles and we can now concentrate on identifying the structural and compositional characteristics of this phase.
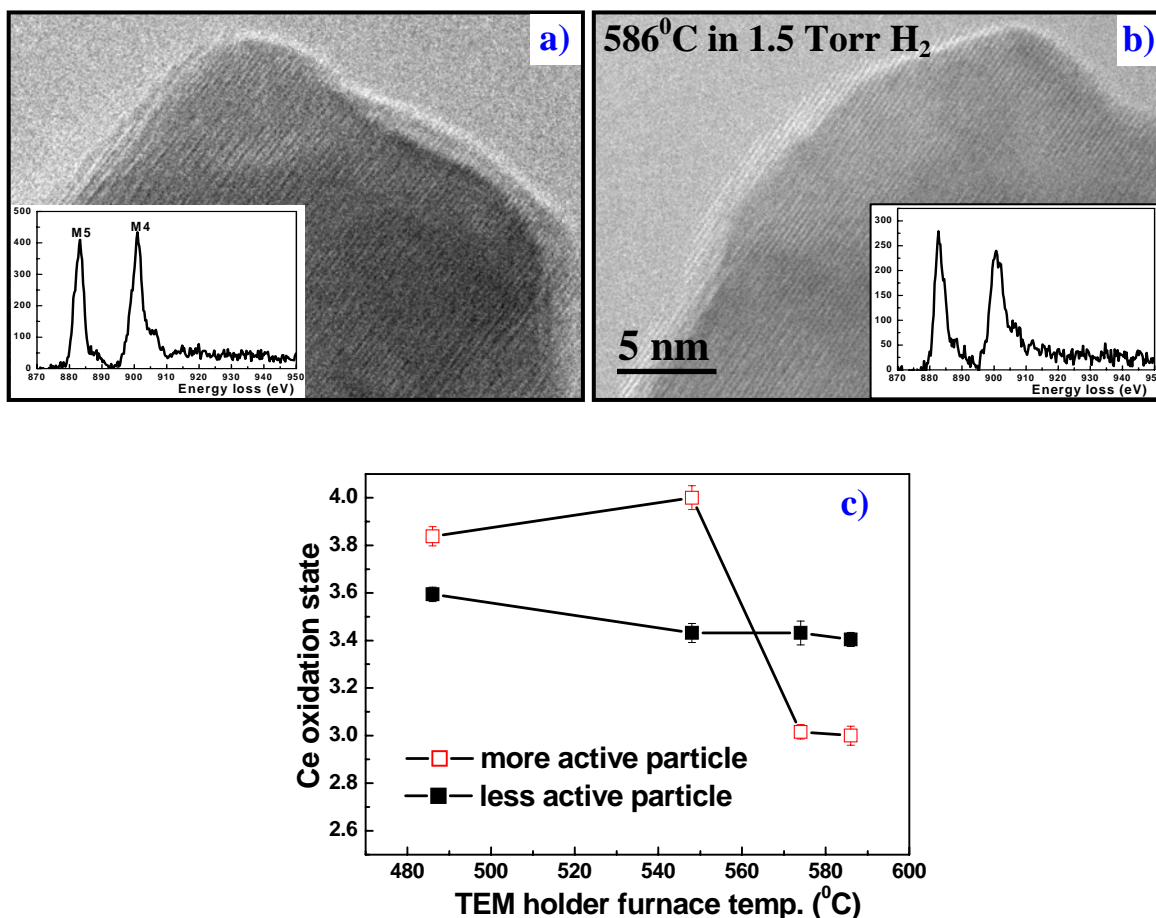


*Figure 4: In situ HREM images from nominally identical nanoparticles of $Ce_{0.5}Zr_{0.5}O_2$ recorded at $586^0C$ in 1.5 Torr $H_2$. The in situ EELS (insert) show that particle (b) is more strongly reduced and active than the particle (a). (c) Oxidation state for same two particles as a function of temperature.*

Figure 5 (a) and (b) show the HREM images of an individual $Ce_{0.5}Zr_{0.5}O_2$ nanoparticle before and after reduction in 1.5 Torr $H_2$ at $472^0C$ and $586^0C$ respectively. The most striking morphological changes, before and after reduction, are located in the areas showing surface

steps or defects indicated by arrow in Figure 5 (a). Nanoparticles have long been used in heterogeneous catalysis to increase the surface area of the catalyst. However, the role of nanoparticles may not be limited to providing a large surface area. Surface steps and defects may play a dominating role in these redox processes. Dahl et al [14], from single crystal experiments, have shown that steps may exhibit up to nine orders of magnitude larger reactivity than the surface facets. The role of nanoparticles may thus include providing a large fraction of particularly active sites (such as steps and defects etc.) and these catalytic active sites will accelerate the oxygen vacancy mobility and improve the low-temperature reducibility. In future experiments, we are expecting to investigate further the role of these defects on the particle reducibility and the difference of activity between the surface facets and defect domains within individual nanoparticles.
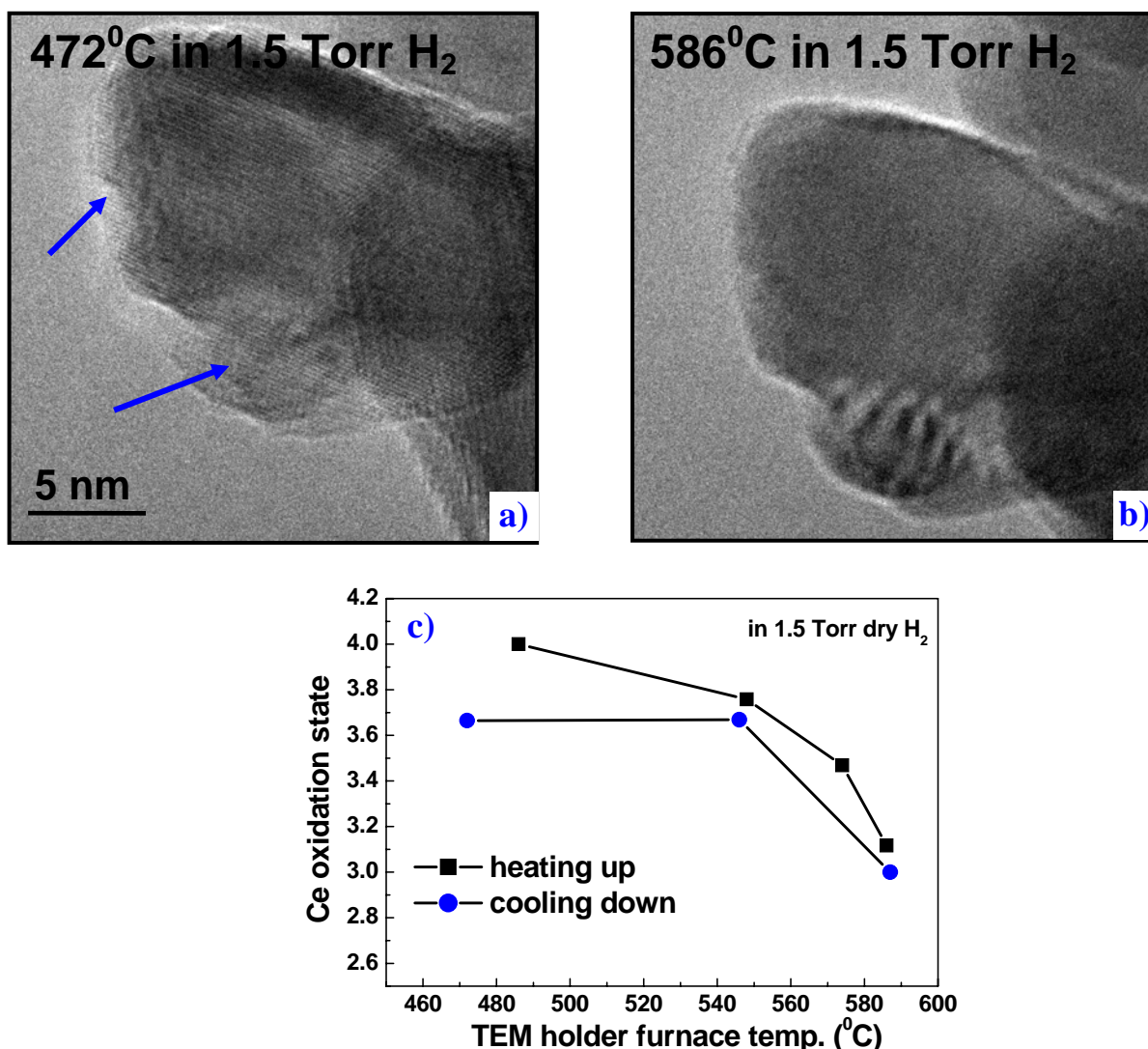


Figure 5: In situ HREM images of one individual ceria zirconia nanoparticle recorded at $472^0C$ (a) and $586^0C$ (b) in 1.5 Torr $H_2$. Hysteresis effect of reduction and oxidation in this nanoparticle is shown in (c).

The Ce oxidation state determined from the Ce $M_{4,5}$ white-line ratio also is plotted as a function of temperature during reduction and oxidation in Figure 5 (c). Starting from the +4 oxidation state at $486^0$, complete reduction (to +3 oxidation state) occurs at about $587^0C$,

which is about $100^0$C higher than *ex situ* dominated reduction temperature ($448^0$C) and $200^0$C lower than *in situ* and *ex situ* reduction temperature ($700\sim800^0$C) for pure $CeO_2$. It should also be noted that the oxidation state for this particle did not completely return to the original +4 state (hysterisis effect), which is consistent with *ex situ* experimental observations and can be due to either oxygen vacancy ordering or the formation of pyrochlore-related phases after reduction. It will be important to establish if these superstructures formed after reduction treatment are active or inactive phases, which requires further *in situ* characterization.

Figure 6 shows an *in situ* HREM image at $586^0$C in 1.5 Torr of dry $H_2$ and associated Ce $M_{4,5}$ spectra from a ceria zirconia nanoparticle during the redox cycle: before reduction at $486^o$C, $586^o$C (reduced) and $472^o$C after spontaneous re-oxidation on cooling. At $586^0$C, local superstructure (oxygen vacancy ordering or intermediate phase) was observed in the reduced nanoparticles (doubling of the $d_{111}$ fluorite spacing). Significant changes in the $M_5/M_4$ intensity ratio of the Ce were not observed until $586^0$C. At this temperature, the $M_5/M_4$ intensity ratio changed from 0.65 ($486^0$C) to $\sim$0.73 ($586^0$C) indicating that a fraction of the $Ce^{+4}$ species transformed to the $Ce^{+3}$ oxidation state. When the sample was cooled to $472^0$C the white-line ratio confirmed the ceria re-oxidation of $Ce^{+3}$ to $Ce^{+4}$, although there was still significant superstructure visible in the micrographs.
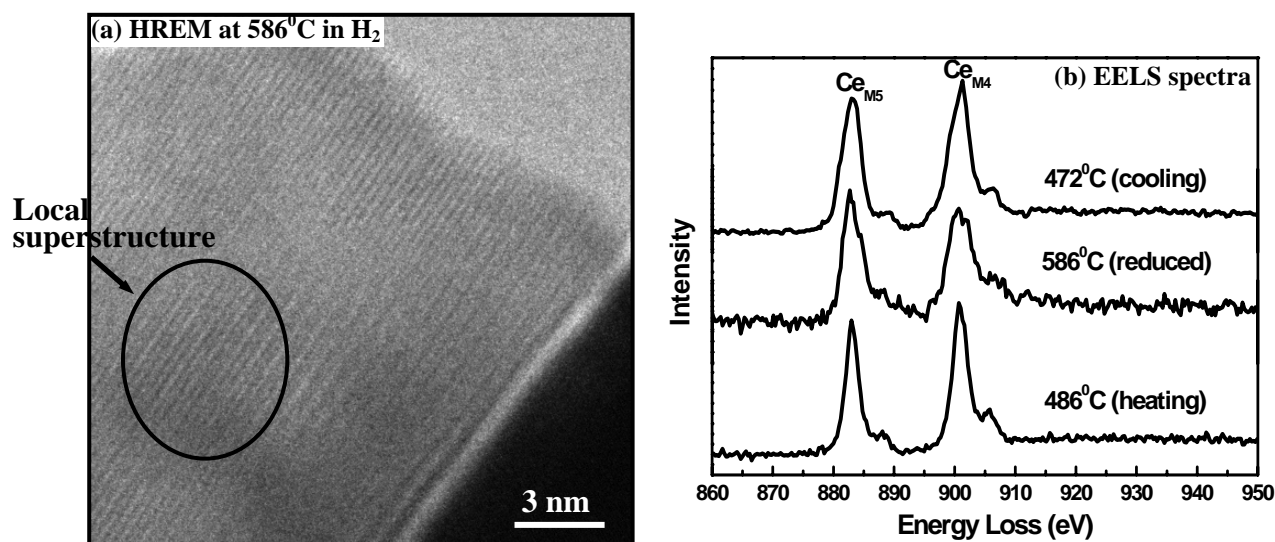


*Figure 6: HREM image recorded at $586^0$C showing doubling of <111> spacing, due to oxygen-deficient phase in 1.5 Torr of $H_2$ (a) and associated EELS spectra (b) during redox process of a $Ce_{0.5}Zr_{0.5}O_2$ naonoparticle*

## Conclusions

We have studied the nanoscale structure and chemistry of individual nominal $Ce_{0.5}Zr_{0.5}O_2$ nanoparticles during *in situ* reduction and oxidation in an environmental TEM. We observed a significant difference of reduction behavior between individual nanoparticles, implying that there are structural and chemical differences in these nanoscale particles. Formation of local superstructure at *in situ* reduction temperature ($576^0$C in 1.5 Torr $H_2$) suggests the importance of oxygen vacancy ordering or pyrochlore-related phases during the reduction processes. However, further *in situ* experiments are necessary to identify these two structures and determine the character with most active nanoparticles.

## Acknowledgement

## References

1. Sharma R., Crozier P.A., Kang Z.C. and Eyring L., Phil. Mag. **84(25-26)** (2004) 2731-2747
2. Fornasiero P., Balducci G., DiMonte R., Kaspar J., Sergo V., Gubitosa G., Ferrero A., Graziani M., J. Catal., **164(1)** (1996) 173-183
3. Montini T., Hickey N., Fornasiero P., Graziani M., Bañares M.A., Martinez-Huerta M.V., Alessandri I., and Depero L.E., Chem. Mater., **17 (5)**(2005) 1157-1166
4. Yeste M.P., Hernández J.C., Bernal S., Blanco G., Calvino J.J., Pérez-Omil J.A, Pintado J.M., Chem. Mater., **18(11)** (2006) 2750-2757
5. Hori C.E., Permana H., Simon Ng K.Y., Brenner A., More K., Rahmoeller K.M., and Belton D., Appl. Catal. B, **16(2)** (1998) 105-117
6. Terribile D., Trovarelli A., Lloreca J., de Leitenburg C., Dolcetti G., Catal. Today, **43(1-2)** (1999) 79-88
7. Alifanti M., Baps B., Blangenois N., Naud J., Grange P., Delmon B., Chem. Mater., **15(2)** (2003) 395-403
8. Rossignol S., Madier Y., Duprez D., Catal. Today, **50(2)** (1999) 261-270
9. Wang R.G., Crozier P.A., Sharma R., Adams J.B., J. Phys. Chem. B, **110 (37)** (2006) 18278-18285
10. Sasaki T., Ukyo Y., Kuroda K., Arai S., Saka H., J. Electron Microsc., **52(3)** (2003) 309-312
11. Sugiura M., Catal. Surveys from Asia, **7(1)** (2003) 77-87
12. Pérez-Omil J.A., Bernal S., Calvino J.J., Hernández J.C., Mira C., Rodríguez-Luque M.P., Erni R., and Browning N.D., Chem. Mater., **17(17)** (2005) 4282 – 4285
13. Kang Z.C., J. Alloys Compd., **408-412** (2006) 1103-1107
14. Dahl S., Logadottir A., Egeberg R.C., Larsen J.H., Chorkendorff I., Törnqvist E., and Nørskov J.K., Phys. Rev. Lett., **83** (1999) 1814–1817